AFRL-MN-EG-TN-2003-7079

Modeling of Fundamentals in Insect Flight

Authors:
H.T. Banks
Emily Ditter

North Carolina State University
Center for Research in Scientific Computation
Box 8205
Raleigh, NC 27695-8205

CONTRACT NO. F08630-00-1-0010

1 December 2002

FINAL REPORT FOR PERIOD June 2000 - December 2001

20030709 041

AIR FORCE RESEARCH LABORATORY, MUNITIONS DIRECTORATE

Air Force Materiel Command ■ **United States Air Force** ■ **Eglin Air Force Base**

NOTICE

WHEN GOVERNMENT DRAWINGS, SPECIFICATIONS, OR OTHER DATA ARE USED FOR ANY PURPOSE OTHER THAN IN CONNECTION WITH A DEFINITE GOVERNMENT-RELATED PROCUREMENT, THE UNITED STATES GOVERNMENT INCURS NO RESPONSIBILITY OR ANY OBLIGATION WHATSOEVER. THE FACT THAT THE GOVERNMENT MAY HAVE FORMULATED OR IN ANY WAY SUPPLIED THE SAID DRAWINGS, SPECIFICATIONS, OR OTHER DATA IS NOT TO BE REGARDED BY IMPLICATION, OR OTHERWISE IN ANY MANNER CONSTRUED, AS LICENSING THE HOLDER, OR ANY OTHER PERSON OR CORPORATION; OR AS CONVEYING ANY RIGHTS OR PERMISSION TO MANUFACTURE, USE, OR SELL ANY PATENTED INVENTION THAT MAY IN ANY WAY BE RELATED THERETO.

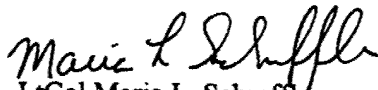## Small Business Innovation Research Program (SBIR)
DATA RIGHTS LEGEND
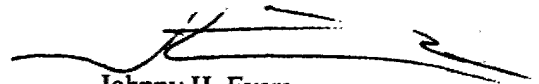Contract Number: F08630-0-1-0010
Contractor: Center for Research in Scientific Research, North Carolina State University

This technical report is releasable to the National Technical Information Services (NTIS). At NTIS it will be available to the general public, including foreign nations.

This technical note has been reviewed for technical content and assessed to be accurate. Due to extenuating circumstances, it is not practical to edit this report for format and it is, therefore, approved "as submitted by the contractor."

LtCol Maria L. Schreffler
Deputy Division Chief
Advanced Guidance Division

Johnny H. Evers
Program Manager
Advanced Guidance Division

Anyone having need of a copy of this report should first contact the Defense Technical Information Center (DTIC) at the address shown below. If you are a registered DTIC User and qualify as a recipient of this document, DTIC can provide you with a copy. Please do not request copies from the Air Force Research Laboratory, Munitions Directorate. Requests for additional copies should be directed to:

Defense Technical Information Center (DTIC)
8725 John J. Kingman Road, Ste 0944
Ft Belvoir, VA 22060-6218

This report is published in the interest of the scientific and technical information exchange. Publication of this report does not constitute approval or disapproval of the ideas or findings. Do not return copies of this report unless contractual obligations or notice on a specific document requires its return. If your address has changed, if you wish to be removed from our mailing list, or if your organization no longer employs the addressee, please notify AFRL/MNG, Eglin AFB FL 32542-6810, to help us maintain a current mailing list. Do not return copies of this report unless contractual obligations or notice on a specific document requires that it be returned..

REPORT DOCUMENTATION PAGE

Form Approved
OMB No. 0704-0188

1. REPORT DATE (DD-MM-YYYY)	2. REPORT TYPE	3. DATES COVERED (From - To)
01-12-2002	Final	16 Jun 2000 – 15 Dec 2001

4. TITLE AND SUBTITLE

Modeling Fundamentals in Insect Flight

5a. CONTRACT NUMBER
F08630-00-1-0010

5b. GRANT NUMBER

5c. PROGRAM ELEMENT NUMBER
61102F

6. AUTHOR(S)

H.T. Banks, Emily Ditter

5d. PROJECT NUMBER
2304

5e. TASK NUMBER
AM

5f. WORK UNIT NUMBER
05

7. PERFORMING ORGANIZATION NAME(S) AND ADDRESS(ES)

North Carolina State University
Center for Research in Scientific Computation
Box 8205
Raleigh, NC 27695-8205

8. PERFORMING ORGANIZATION REPORT NUMBER

9. SPONSORING / MONITORING AGENCY NAME(S) AND ADDRESS(ES)

AFRL/MNGN
101 West Eglin Blvd., Suite 329
Eglin AFB, FL 32542-6810

10. SPONSOR/MONITOR'S ACRONYM(S)

11. SPONSOR/MONITOR'S REPORT NUMBER(S)
AFRL-MN-EG-TN-2003-7079

12. DISTRIBUTION / AVAILABILITY STATEMENT

DISTRIBUTION Approved for public release; distribution is unlimited.

13. SUPPLEMENTARY NOTES

14. ABSTRACT
The objective of this study is to represent large data fields with a reduced set of data using Proper Orthogonal Decomposition (POD). The original effort focused on reduced order modeling for a set of aerodynamics data for an experimental flapping wing. Due to delays in obtaining an adequate data set with which to demonstrate the POD methodology, the project was refocused on a similar modeling problem involving reconstruction of human nasal airway passages, since that data set was readily available. This report describes the POD approach utilized in the study.

15. SUBJECT TERMS
Proper orthogonal decomposition, elementary motion detection, insect vision, motion processing, insect neurobiology, vision circuits.

16. SECURITY CLASSIFICATION OF:			17. LIMITATION OF ABSTRACT	18. NUMBER OF PAGES	19a. NAME OF RESPONSIBLE PERSON Johnny H. Evers
a. REPORT	b. ABSTRACT	c. THIS PAGE			19b. TELEPHONE NUMBER (include area code)
U	U	U	UL	35	(805) 882-2220 x3330

Standard Form 298 (Rev. 8-98)
Prescribed by ANSI Std. Z39.18

Modeling of Fundamentals in Insect Flight

Final Technical Report

for the period

June 16, 2000 – December 15, 2001

Grant USAF # F08630-00-1-0010

Principal Investigator

Dr. H.T. Banks
North Carolina State University
Center for Research in Scientific Computation
Box 8205
Raleigh, NC 27695-8205
htbanks@eos.ncsu.edu

Project Manager

Johnny H. Evers
AFRL/MNGN
101 W. Eglin Blvd. Ste. 329
Eglin AFB, FL 32542-6810
Ph. (850) 882-2220 ext. 2347
johnny.evers@eglin.af.mil

Summary of Efforts

The general focus of this effort involved investigation of sensory processing, navigation, guidance and motion control mechanisms that are the basis of insect flight. The effort utilized modeling, data analysis and simulation in an attempt to develop basic paradigms and models with attention to the possibility of using similar paradigms in the design of autonomous flying vehicles.

A large body of literature on insect flight indicates that insects utilize unsteady aerodynamics to achieve flight performance beyond that predicted from classical aerodynamics theory. Aerodynamic models have not yet been developed from the abundant force and moment data that has been collected from tethered flying insects or from hardware models that replicate the kinematics of insect flapping. These models which most likely will involve flight dependent parameters (lift, drag) in an innovative manner, are essential for simulating flapping flight and for developing an understanding of the incredible robustness evident in insect flight response. The research entailed initial efforts on development of an aerodynamics model, suitable for eventual simulation of insect flight, based upon existing force and moment data taken in the Dickinson lab at UC Berkeley The huge DoD investments in micro air vehicles that utilize micro-sensors and actuators for active flow control motivate research extending our understanding of how insects exploit unsteady aero for flight.

Insects exhibit extraordinary navigation, guidance, and control capabilities in their free flight response to visual stimuli. On going research in this area (e.g., Dickinson), and in insect gaze stabilization during flight (e.g., Gilbert), involves reconstruction of free flight trajectories from 3D high-speed video. Although biologists are a long way from obtaining sufficient neurophysiological data for developing a detailed understanding of the guidance and control system design features of insects, the flight trajectory data may be used to infer models that represent free flight response. This research area involves development of guidance models from the recent high quality trajectory data and making comparisons with those previously reported in the biological literature (e.g., Ohlberg).

During the early phases of the research period, the investigators collaborated with J. Evers and his associates in considering the above aspects of insect flight modeling. A determination of priorities and feasibilities was made, after which specific efforts focused on detailed investigations.

During the summer of 2000, Emily Ditter (the graduate student supported by this grant) began working with H.T. Banks to model the forces generated by the flapping wings of fruit flies as part of an on-going United States Air Force project. Johnny Evers at Eglin Air Force Base in Florida had been working with Dr. Michael H. Dickinson (University of California, Berkeley) to determine this model for implementation in the design of unmanned air vehicles.

Her efforts began with a 6 week stay at Eglin Air Force Base to conduct research jointly with J. Evers and study the data provided by Dr. Dickinson. After studying fruit flies, Dr. Dickinson and his team developed a robotic fruit fly wing that was suspended in oil. This wing replicated the kinematics of the fruit fly wing, enabling force measurement data collection using sensors placed about the wing. Dr. Dickinson measured the forces for several different wing beat scenarios and forwarded the data to us.

Our efforts began by studying the actions of the fruit fly wing, trying to incorporate as much of the real life movement into our model as possible. The fruit fly's wing sweep is actually quite complicated in that it is not just a back and forth motion. The wing sweeps forward, and upon reaching the front of the fly, rotates and sweeps backward again. The fly is in control of when this rotation happens and at what angle and speed it rotates. The fly can also sweep its wings at varying speeds, angles, and lengths of arcs. We felt that all of these factors and their interdependence were important in developing our model.

We created a model that looked at the changes of lift and drag as a function of eight different parameters. These parameters depended on the angles subtended and the angular velocities of the wing. We developed code in Matlab to represent this model and performed optimization simulations on the parameters to fit the experimental data. Unfortunately, the optimum parameter set did not accurately represent the data, leading us to pursue an alternative approach. This consisted of a model reduction approach based on experimental data.

We focused on an approach called Proper Orthogonal Decomposition (POD). Mathematicians and scientists have used POD in a number of different applications such as fluid flow analysis and the modeling of thin film formation using Chemical Vapor Deposition. We hoped to retrieve supplemental data from Dr. Dickinson that would show the force fields generated by the wings, allowing us to use POD to create a reduced order model of these force fields.

While waiting for this data, we decided to test the POD approach on a similar set of data (that was *readily available*) involving flow in a constrained passage way. We obtained data that consisted of many sets of nasal airway passage cross-sections of rhesus monkeys. This study was successfully completed and its results are given in the M.S. project paper, "Representation of Nasal Airways Using Proper Orthogonal Decomposition" by E. Ditter. In the study, we demonstrated nasal airways can be represented by a small number of orthogonal components, thereby giving a model for the airway that is smaller and easier to deal with than the entire system. Details of the approach and specific results are given in the report attached as Appendix 1.

Although suitable fruit fly data was not obtained during the course of our efforts, we believe that POD may be a viable approach to modeling the flight of fruit flies and should be pursued in the future.

Representation of Nasal Airways Using Proper Orthogonal Decomposition

E. E. Ditter

G. M. Kepler

R. Guilmette

H. T. Banks

April 2002

Contents

List of Figures

List of Tables

Acknowledgements

1 Introduction

Working with images often requires the use of large fields of data. The objective of this study is to represent large data fields with a reduced set of data using Proper Orthogonal Decomposition (POD). POD has been previously used by M. Kirby and L. Sirovich to study patterns that occur in images of human faces [9, 13]. This study implements POD to reconstruct human nasal airways.

2 Nasal Airway Data

Nasal airways can be visualized through a series of two dimensional cross sections taken throughout the air passage. Actual cross sections are obtained using Magnetic Resonance Imaging (MRI) technology. In humans, the nasal passage is separated by the septal wall, which extends from the nostrils to the pharynx. The septal wall separates the right and left airways, which are almost mirror images of each other. The wall ends at the pharynx, where the two airways join to form one. At the nostrils, the cross sections are close to oval in shape. As one travels through the airways toward the pharynx, the cross sections elongate and individualize. (see Figure 1.)

Airflow and absorption patterns are intimately connected to nasal shape [10, 6, 14], therefore, a method for describing nasal shape is needed. In the future this method may be used to help identify subpopulations through correlations between nasal shape data and predicted susceptibility to inhaled toxicants.

2.1 Data Description

Two dimensional cross sections (as depicted in Figure 1) were obtained from seven male and seven female nonsmoking adults. Each subject contained a different number of cross sections as shown in
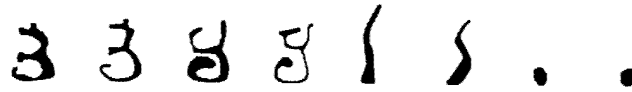
Figure 1: Alternating right and (flipped) left airway cross sections from Sample 02. The first and second cross sections are the right and left airways at the pharynx, respectively. The third through sixth cross sections are of the airway between the pharynx and the nostril. Cross sections seven and eight are the right and left airways at the nostril, respectively. Cross sections shown are eight out of fifty-four available sections of Sample 02. (Left cross sections have been flipped for comparison purposes.)

Table 1. The collection of cross sections from one subject will be referred to as a sample.

Table 1: Number of cross sections per sample

Sample	Cross-sections
02	54
03	58
06	56
07	56
08	54
09	50
10	52
12	44
14	60
15	52
16	56
17	56
18	58
19	52

The acquired MRI images were hand digitized from the gray scale images and stored as 3D coordinate data. For comparison among individuals, the original (xyz) coordinate data for each cross section was translated and scaled to nondimensianal $(x'y'z')$ coordinates.

$$x' = \frac{(x - x_0)}{2W}, \; y' = \frac{(y - y_0)}{H}, \; and \; z' = \frac{z}{L} \tag{1}$$

2

where the values of W, H, and L were determined for each subject: L was the length of the septal wall, W was the maximum width among the cross sections, and H was the height among cross sections. The translation values x_0 and y_0 corresponded to the minumum x and y coordinates within each right or (flipped) left cross section. For each subject, the relative size among cross sections was maintained, though the aspect ratio was changed. The relative size among subjects was not maintained. Values for W, H, and L are shown in Table 2.

Table 2: Subject gender and scaling data

Sample	W (mm)	H (mm)	L (mm)	Gender
02	14.0	43.3	78	male
03	13.6	45.9	84	male
06	18.9	53.0	81	male
07	17.7	47.1	81	male
08	15.5	41.6	78	male
09	17.0	39.1	75	female
10	17.3	38.8	75	female
12	15.9	43.2	63	female
14	18.1	50.6	87	male
15	14.4	42.0	75	female
16	18.1	44.6	81	female
17	18.4	49.7	84	male
18	??	??	??	??
19	15.9	49.6	75	female

Each cross section is a 75 × 150 array of binary data which is viewed on the plots in black and white. Each element of this data will be referred to as a pixel.

3 Method

Proper Orthogonal Decomposition, also known as Principal Component Analysis and Karhunen-Loève Expansion, is a method used to represent large (possibly nonlinear) data fields with a rela-

tively small number of elements. Proper Orthogonal Decomposition creates a basis set which spans the original data set by capturing the characteristic elements of the data. The majority of these characteristics are usually captured in the first few POD elements, and therefore, the data system can often be represented well by these first few elements.

Proper Orthogonal Decomposition has been used with many different applications including Chemical Vapor Decomposition Reactors [3, 7, 8, 12], Raleigh-Bérnard Convection [11], open cavity acoustics [4], evaluation of material integrity [2], control of beam vibrations [5] and characterization of human faces [9, 13].

3.1 Mathematical Background

The data must be gathered in snapshots. A snapshot is a single set of data at a certain physical parameter (time, distance, Reynolds number, etc.). For our purposes, snapshots will be taken three millimeters apart. Each snapshot appears as a cross section. Let $\{U_i(x) : 1 \leq i \leq N, x \in \Omega\}$ be the set of N snapshots on the domain Ω. The average of the snapshots is given by:

$$\bar{U} = \frac{1}{N} \sum_{i=1}^{N} U_i(x) \tag{2}$$

We concentrate on each snapshot's deviation from the average, since this leads to a more efficient approach, and follows the procedure of past works [9, 13, 11]. Our new snapshots, W_i, $i = 1, \ldots, N$, are:

$$W_i = U_i - \bar{U}, \quad \forall \ i = 1, \ldots, N \tag{3}$$

We want to form POD basis elements which most closely resemble our snapshots in the L^2 sense that

$$\frac{1}{N} \sum_{i=1}^{N} |(W_i(x), \Phi)|^2 \tag{4}$$

4

is maximized, subject to $(\Phi, \Phi) = ||\Phi||^2 = 1$. Note that $(\cdot, \cdot)$ and $|| \cdot ||$ are respectively the L^2 inner product and norm over Ω. We choose the following for the POD basis elements:

$$\Phi = \sum_{i=1}^{N} a_i W_i \tag{5}$$

where a_i, $i = 1, 2, ..., N$, are chosen such that Φ maximizes equation (4).

We define, as in [12],

$$K(x,y) := \frac{1}{N} \sum_{i=1}^{N} W_i(x)W_i(y) \ \ and \ R\Phi := \int_{\Omega} K(x,y)\Phi(y)dy,$$

where $R : L^2 \to L^2$. Then we find that

$$
\begin{aligned}
(R\Phi, \Phi) &= \int_{\Omega} R\Phi(x)\Phi(x)dx \\
&= \int_{\Omega} \int_{\Omega} K(x,y)\Phi(y)dy\,\Phi(x)dx \\
&= \frac{1}{N} \sum_{i=1}^{N} \int_{\Omega} \int_{\Omega} W_i(x)W_i(y)\Phi(y)dy\,\Phi(x)dx \\
&= \frac{1}{N} \sum_{i=1}^{N} |(W_i, \Phi)|^2
\end{aligned}
$$

Furthermore,

$$(R\Phi, \Psi) = (\Phi, R\Psi), \quad \forall\, \Phi, \Psi \in L^2$$

Since R is a nonnegative symmetric operator on $L^2(\Omega)$, we can compare the problem of maximizing the quantity (4) to maximizing the eigenvalue problem $R\Phi = \lambda\Phi$, subject to $||\Phi||^2 = 1$.

$$
\begin{aligned}
\max \frac{1}{N} \sum_{i=1}^{N} |(W_i(x), \Phi)|^2 &= \max(R\Phi, \Phi) \\
&= \max(\lambda\Phi, \Phi) \\
&= \max \lambda||\Phi|| \\
&= \max \lambda
\end{aligned}
$$

So, we are seeking the maximum eigenvalue to the eigenvalue problem $R\Phi = \lambda\Phi$ subject to $\|\Phi\| = 1$.

Therefore,

$$\lambda\Phi = R\Phi = \int_\Omega K(x,y)\Phi(y)dy \tag{6}$$

Substituting equation (5) and the definition of K into equation (6), we have:

$$\int_\Omega \frac{1}{N}\sum_{i=1}^N W_i(x)W_i(y)\Phi(y)dy \ = \ \lambda\sum_{i=1}^N a_i W_i(x)$$

$$\int_\Omega \frac{1}{N}\sum_{i=1}^N W_i(x)W_i(y)\sum_{k=1}^N a_k W_k(y)\ dy \ = \ \lambda\sum_{i=1}^N a_i W_i(x)$$

$$\sum_{i=1}^N \left[\sum_{k=1}^N \left(\frac{1}{N}\int_\Omega W_i(y)W_k(y)\ dy\ \right)a_k\right] W_i(x) \ = \ \lambda\sum_{i=1}^N a_i W_i(x)$$

We can rewrite this as another eigenvalue problem $CV = \lambda V$, where

$$C_{ik} \ = \ \frac{1}{N}\int_\Omega W_i(y)W_k(y)dx \ \ and \ \ V \ = \ \begin{bmatrix} a_1 \\ \vdots \\ a_N \end{bmatrix}$$

The covariance matrix, C, is a nonnegative Hermitian matrix [1] and has a complete set of orthogonal eigenvectors,

$$V^1 \ = \ \begin{bmatrix} a_1^1 \\ \vdots \\ a_N^1 \end{bmatrix}, \ V^2 \ = \ \begin{bmatrix} a_1^2 \\ \vdots \\ a_N^2 \end{bmatrix}, \ \ldots, \ V^N \ = \ \begin{bmatrix} a_1^N \\ \vdots \\ a_N^N \end{bmatrix}$$

with corresponding real eigenvalues, $\lambda_1 \geq \lambda_2 \geq \cdots \geq \lambda_N \geq 0$. Therefore, our first POD element is given by:

$$\Phi_1 \ = \ \sum_{i=1}^N a_i^1 W_i \tag{7}$$

where a_i^1 are elements of the first eigenvector, V^1. The remaining POD elements, $\Phi_i, i = 2,\ldots,N$ are obtained by using elements from the remaining eigenvectors, $V^i, i = 2,\ldots,N$.

If we want our POD elements to form an orthonormal basis set, we must impose the following normalizing condition on the eigenvectors:

$$V^k \cdot V^j = \sum_{i=1}^{N} a_i^k a_i^j = \begin{cases} \frac{1}{N\lambda_k}, & k = j \\ \\ 0, & k \neq j \end{cases} \qquad (8)$$

Using our imposed condition (8), we can show that the Φ_i's are orthonormal.

$$
\begin{aligned}
(\Phi_k, \Phi_{k'}) &= \int_{\Omega} \Phi_k(x)\Phi_{k'}(x)dx \\
&= \int_{\Omega} \sum_{i=1}^{N} a_i^k W_i(x) \sum_{j=1}^{N} a_j^{k'} W_j(x)dx \\
&= \sum_{i=1}^{N} a_i^k N \sum_{j=1}^{N} \left(\frac{1}{N} \int_{\Omega} W_i(x)W_j(x)dx \right) a_j^{k'} \\
&= \sum_{i=1}^{N} a_i^k N \sum_{j=1}^{N} C_{ij} a_j^{k'} \\
&= N V^k \cdot C V^{k'} \\
&= N \lambda_{k'} V^k \cdot V^{k'} \\
&= \begin{cases} 1 & k = k' \\ \\ 0 & k \neq k' \end{cases}
\end{aligned}
$$

Therefore, as long as condition (8) is met, $\{\Phi_i\}$ is an orthonormal basis set.

3.2 Implementation

In order to perform POD on our nasal cross section images, we must first assemble the snapshots into an easily accessible matrix. We will call this collection of snapshots U. Each snapshot is essentially a matrix itself (comprised of binary entries) being 75×150 pixels. We concatenate the rows of the

snapshot and transpose them to place in one column of U. Using P as the number of snapshots (cross sections) in a certain sample, and having 11,250 pixels per snapshot, we form an $11,250 \times P$ matrix, U, which contains all of the snapshots from one sample.

Now that we have assembled all of our snapshots, we can easily calculate the average of each row using equation (2) and then form our new snapshots, W_i, $i = 1, \ldots, N$, using equation (3).

The next step is to construct the matrix C so that we can find the eigenvectors and eigenvalues for the problem $CV = \lambda V$. Because we have distinct values and not a continuous function,

$$C_{ik} = \frac{1}{N} \int_{\Omega} W_i(x) W_k(x) dx$$

is equivalent to

$$C_{ik} = \frac{1}{N} \left(W_i(x) \cdot W_k(x) \right)$$

We then solve the eigenvalue problem, finding both the eigenvectors, V^i, $i = 1, \ldots, N$, and their corresponding eigenvalues, λ_i, $i = 1, \ldots, N$, in descending order. We will see later why the order is important.

Once we have our eigenvectors, $\{V^i\}$, we scale them using the following formula:

$$V^i = \frac{1}{\sqrt{N \times \lambda_i}} V^i, \quad \forall\, i = 1, \ldots, N$$

This ensures that the imposed condition (8) holds, and therefore our POD basis elements will form an orthonormal set.

Now, we need to find our POD basis elements, Φ_i, $i = 1, \ldots, N$. Using equation (7), the first POD element is given by:

$$\Phi_1 = \sum_{i=1}^{N} a_i^1 W_i$$

The other elements, Φ_i, $i = 2, \ldots, N$, are calculated in a similar manner. Once we have all N POD elements we can start reconstruction of the cross sections.

8

3.3 Reconstruction

Any snapshot, U^j, can now be reconstructed using a linear combination of our POD basis elements.

$$U^j = \bar{U} + \sum_{k=1}^{N} \alpha_k^j \Phi_k \tag{9}$$

with

$$\alpha_k^j = \Phi_k \cdot W_j \tag{10}$$

The above equations (9) and (10) will represent the snapshots exactly. Now we look at the error created by truncating the series in equation (9).

3.4 Error

If we use an approximation to equation (9)

$$U_M^j = \bar{U} + \sum_{k=1}^{M} \alpha_k^j \Phi_k \tag{11}$$

where $M << N$, we have introduced an error into our reconstruction. The error is calculated as follows:

$$Error = \frac{||U - U_M||}{||U||}$$

or

$$\% \, Error = \frac{number \ of \ pixels \ incorrect}{total \ number \ of \ pixels} \times 100 \tag{12}$$

3.5 Density

We need a method to discover an acceptable M in equation (11) before we run all of our calculations. We want (11) to be a good approximation to (9). In previous studies of fluid flow [4, 12] the data fields analyzed are fields of velocities. When constructing a sum of the squares of these velocities,

9

the author creates a formula akin to kinetic energy. We would like to study a comparable quantity in our observations of the fields of binary data representing nasal cross sections. We will use the same type of analysis as found in [4, 12], but will refer to our function as *Density*.

The density of the system is a way to measure an acceptable M quantitatively. Density is calculated using the following formula:

$$\% \ Density \ = \ \frac{\sum_{i=1}^{M} \lambda_i}{\sum_{i=1}^{N} \lambda_i} \times 100 \qquad (13)$$

where M is the number of POD elements used and N is the total number of POD elements available. The λ_is are the eigenvalues associated with the POD eigenvectors. Since we have ordered the eigenvalues with the largest first, we capture most of the density in the first few eigenvalues, and therefore in the first few POD elements.

4 Results

When the regeneration of the data takes place, each pixel is returned with a grey scale value, i.e. each pixel value $\in [0,1]$. This must be converted to a black or white value in binary form. If the pixel returns a value less than 0.5, it is assigned a value of 0. If the returned value is greater than or equal to 0.5, it is assigned a value of 1.

All results are calculated on a Windows station with a Pentium II processor using Matlab 5.3.1.

4.1 Regenerating Sample 02 Using Its Own POD Elements

The first analysis consisted of using POD on the cross sections of Sample 02 and regenerating that same sample. A total of fifty-four snapshots were available in the sample. Variable numbers of POD elements were used to regenerate the data (54, 40, 30, 20, 10 and 5) and the density was calculated.
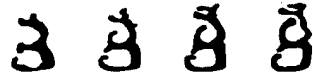
10

Figure 2: Sample 02 - Original snapshots

Figure 3: Sample 02 - Reconstruction using 54 elements

The time shown is the time to construct POD elements, calculate density and reconstruct the data. The construction of the POD elements takes 117 seconds. Results follow in Table 3. Figure 2 shows the first four cross sections of Sample 02. Figures 3 - 6 show the first four snapshots represented by 54, 40, 20 and 5 elements, respectively. Notice that we cannot see much of a difference between the original snapshots and the reconstruction of Sample 02 until we are only using five elements. Using five elements cuts the processing time by forty-six percent. In a larger problem, this could be a significant decrease in computing time.

Table 3: Sample 02

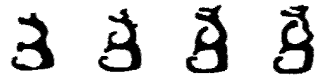| No. of elements	Density (%)	Time (sec.)	Error (%)
54	100.00	225.36	0.00
50	99.52	214.76	0.003
40	96.10	194.32	0.105
30	89.88	174.50	0.369
20	80.16	153.85	1.4171
10	63.35	133.80	4.377
5	47.36	123.47	7.507

11

Figure 4: Sample 02 - Reconstruction using 40 elements

Figure 5: Sample 02 - Reconstruction using 20 elements

4.2 Base Sets

In order to determine if the population can be represented adequately by a smaller set of data, we choose a small number (four, five, or six) of the samples to construct a base set. POD is performed on the collection of snapshots from the chosen samples to form a base set of N snapshots. In this paper, we use four different base sets.

The bases formed by implementing POD on each of the base sets were used to regenerate the fourteen sets of data using:

1. all available POD elements (100% density)

2. enough POD elements to capture 90% of the density

3. ten percent of the POD elements (variable density)

Figure 6: Sample 02 - Reconstruction using 5 elements

12

The following tables (Tables 4-7) show the Total Error, Average Error, Density, and Time. The Total Error is the sum of the errors generated by using N (or M) of the available POD elements to regenerate each of the fourteen Samples. The Average Error is the average of the errors when regenerating all of the Samples using N (or M) of the available POD elements to regenerate each sample. The Density is defined by equation (13). The Time is the time to construct the POD elements, read in the Sample 14 file and reconstruct and plot the regenerated Sample 14. (Sample 14 is used as an example so that the reader can experience the regeneration of a sample visually.)

4.2.1 Base Set 1

Base Set 1 consisted of Samples 02, 03, 12 and 18 for a total of 214 snapshots. The implementation of POD on Base Set 1 constructed $N = 214$ POD elements, which were then used to reconstruct each sample. First, all of the 214 POD elements were used (100% density). Then eighty-six POD elements were used (90% density). Finally, ten percent, or twenty-one POD elements, were used to reconstruct the samples. The results are shown in Figure 7 and Table 4. The generation of all 214 POD element took 2821 seconds. Using Sample 14 as an example, the original snapshots and reconstructed snapshots are shown in Figures 8-10.

We can see that using only twenty-one POD elements yields an image that is significantly different than the original. However, using eighty-six POD elements is only slightly different, with an error of 3.35%. Using eighty-six POD elements reduces the computational time by 54%.

Table 4: Base Set 1

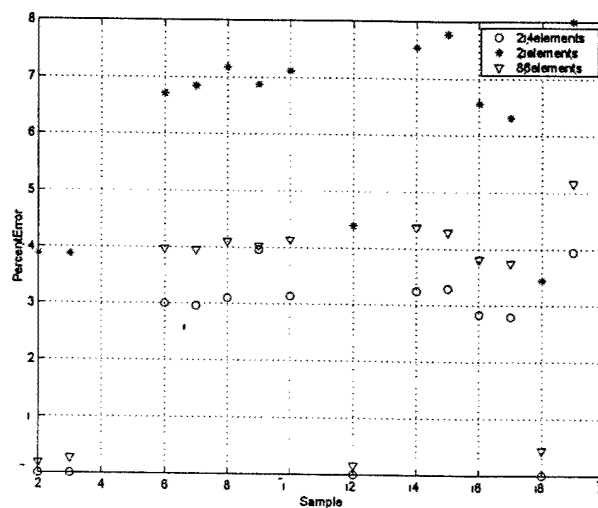| Elements	Total Error(%)	Average Error(%)	Density (%)	Time (sec.)
N=214	32.29	2.31	100	7021
M=21	86.41	6.17	65	3221
M=86	42.69	3.05	90	3852

Figure 7: Base Set 1

Figure 8: Sample 14 - Original snapshots

Figure 9: Sample 14 - Reconstruction using 214 POD elements of Base Set 1

Figure 10: Sample 14 - Reconstruction using 86 POD elements of Base Set 1

14

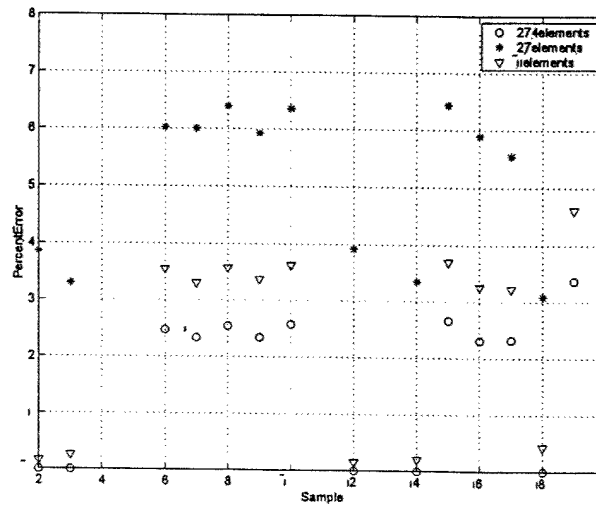Figure 11: Sample 14 - Reconstruction using 21 POD elements of Base Set 1

Figure 12: Base Set 2

4.2.2 Base Set 2

Base Set 2 consisted of samples 02, 03, 12, 14, and 18 for a total of 274 snapshots. The POD of Base Set 2 resulted in a total of $N = 274$ POD elements (which took a total of 6805 seconds to generate). The results are shown in Figure 12 and Table 5. Figures 13 - 10 show the first four reconstructed cross sections of Sample 14.

Using twenty-seven POD elements generates a visual difference that is slightly different from the original, with only 7.54% error. Reconstruction using twenty-seven POD elements reduces the time by 78%.

Figure 13: Sample 14 - Original snapshots

16

Table 5: Base Set 2

Elements	Total Error(%)	Average Error(%)	Density (%)	Time (sec.)
N=274	22.95	1.64	100	31949
M=27	73.62	5.26	68	7105
M=101	33.42	2.39	90	8461

Figure 14: Sample 14 - Reconstruction using 274 POD elements of Base Set 2

4.2.3 Base Set 3

Base Set 3 consisted of Samples 02, 03, 12, 14, 18 and 19 totaling 326 snapshots. Performing POD on Base Set 3 resulted in a total of $N = 326$ POD elements, which took 13,224 seconds to generate. The results are shown in Figure 17 and Table 6. Figures 18 - 20 are the first four reconstructed cross sections of Sample 14.

Reconstruction of Sample 14 does not show a visual difference until we use only thirty-three POD elements. The error here is 3.02% while the time is reduced by 88%.

Table 6: Base Set 3

Elements	Total Error(%)	Average Error(%)	Density (%)	Time (sec.)
N=326	16.61	1.19	100	119640
M=33	62.99	4.50	69	14608
M=115	25.85	1.85	90	17946

Figure 15: Sample 14 - Reconstruction using 101 POD elements of Base Set 2

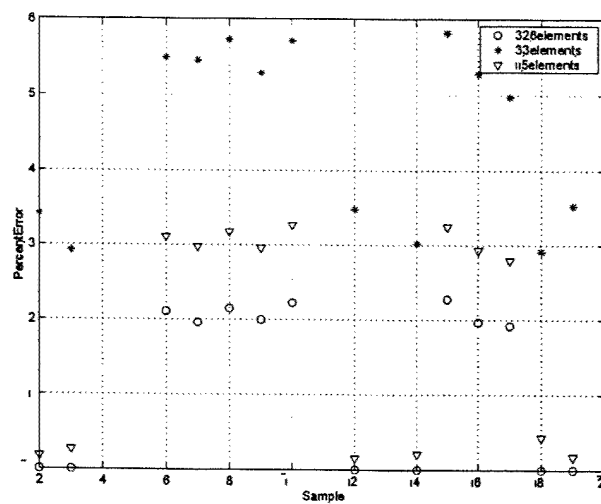Figure 16: Sample 14 - Reconstruction using 27 POD elements of Base Set 2

Figure 17: Base Set 3

Figure 18: Sample 14 - Original snapshots

18

Figure 19: Sample 14 - Reconstruction using 326 POD elements of Base Set 3

Figure 20: Sample 14 - Reconstruction using 115 POD elements of Base Set 3

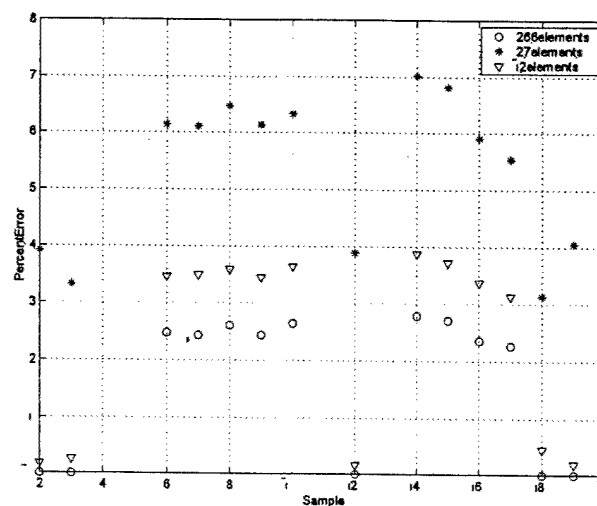Figure 21: Sample 14 - Reconstruction using 33 POD elements of Base Set 3

Figure 22: Base Set 4

4.2.4 Base Set 4

Base Set 4 consisted of Samples 02, 03, 12, 14, and 19 totaling 266 snapshots. The POD resulted in a total of $N = 266$ POD elements, which took 6,034 seconds to generate. The results are shown in Figure 22 and Table 7. Figures 23 - 25 show the reconstructed first four cross sections of Sample 14.

In this Base Set, we cannot see a visual difference until we are only using twenty-seven POD elements. By using twenty-seven POD elements, we reduce the time by 32%, but increase the error by only 7.02%.

Table 7: Base Set 4

Elements	Total Error(%)	Average Error(%)	Density (%)	Time (sec.)
N=266	22.73	1.62	100	9689
M=27	74.78	5.34	67	6606
M=102	32.97	2.35	90	7407

20

Figure 23: Sample 14 - Original snapshots

Figure 24: Sample 14 - Reconstruction using 266 POD elements of Base Set 4

Figure 25: Sample 14 - Reconstruction using 102 POD elements of Base Set 4

Figure 26: Sample 14 - Reconstruction using 27 POD elements of Base Set 4

5 Reconstructions Based on Error

To determine whether the samples provided can be reconstructed within reason, an error tolerance must be set. Since the particular use of the POD technique will dictate the resolution desired in reconstruction, it can be expected that different tolerances might be required in various applications. To illustrate the POD capabilities at one level, we choose an error (as defined in equation 12) of 5% as acceptable.

5.1 Using Base Sets to Reconstruct Each Sample

POD elements generated from the four different base sets are used to represent each of the fourteen samples. The number of elements needed from each base set to reconstruct the samples within the stated error tolerance are plotted on Figure 27.

Upon reconstruction of the data, it was observed that when the snapshots from a certain sample are used to form the Base Set, it takes less elements from that Base Set to reconstruct that sample. For example, the snapshots from Sample 19 are used to form Base Set 3 and Base Set 4. We can see from Figure 27 that it takes twenty-six elements from Base Set 3 and twenty-three elements from Base Set 4 to reconstruct Sample 19 within the tolerance. However, it takes ninety-four elements from Base Set 1 and eighty elements from Base Set 2 to meet the error criterion when reconstructing Sample 19.

5.2 Using Each Sample to Reconstruct Itself

In this experiment, each sample is used as its own Base Set. For example, POD is performed on the cross sections from Sample 02. The basis that is formed is used to reconstruct Sample 02. This is then repeated for each of the other thirteen samples. The number of basis elements needed to
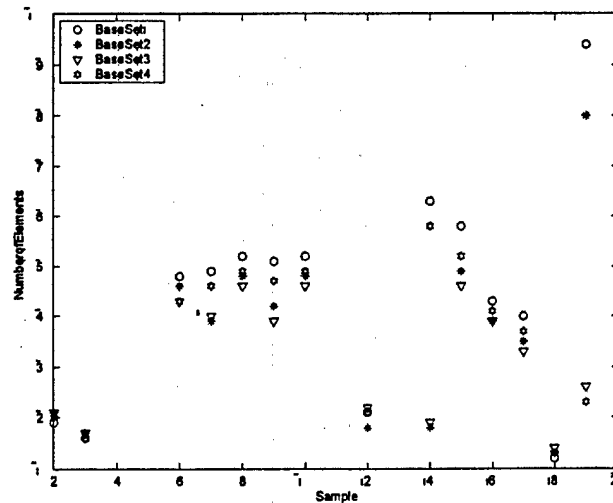
Figure 27: Base sets 1-4 reconstructing each sample

reconstruct the original cross sections within the error tolerance is determined and the results are shown on Figure 28.

An average of eight POD elements are needed to reconstruct each sample with its own Base Set within the error tolerance. (There is an average of fifty-four POD elements constructed in each Sample.) Less than twenty percent of the available POD elements are needed on average to reconstruct the samples.

6 Conclusions

As one might expect, fewer elements are needed to represent the samples that are in the Base Set as compared to the samples outside of the Base Set. As more snapshots are added to a Base Set, it becomes easier to represent a Sample. However, adding more snapshots increases the computing
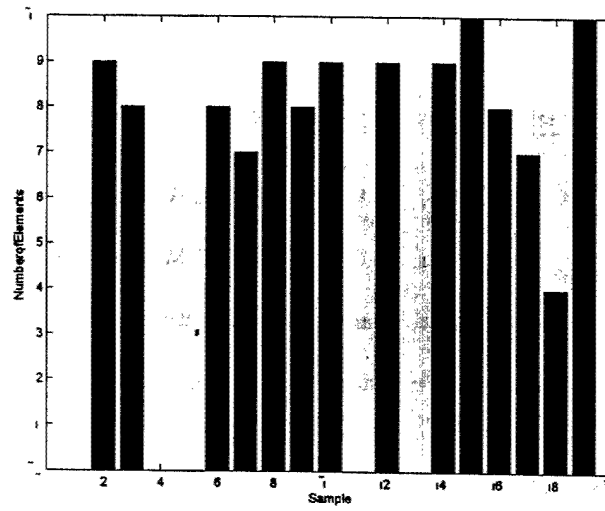
23

Figure 28: Number of elements from each sample needed to reconstruct its own cross sections with less than 5% error.

time. Therefore, we need a well chosen Base Set to represent the field of data.

We have shown that Proper Orthogonal Decomposition can be an effective tool to represent human nasal cross sections with an error tolerance specified by the user. With an acceptable error of 5%, each of the fourteen samples was represented with less than half of the available POD elements.

24

References

[1] Anton, H. _Elementary Linear Algebra 5e_. New York: John Wiley and Sons, 1987.

[2] H.T. Banks, M.L. Joyner, B. Wincheski, and W.P. Winfree. "Evaluation of Material Integrity Using Reduced Order Computational Methodology." Center for Research in Scientific Computation, North Carolina State University, Technical Report CRSC-TR99-30, _http://www.ncsu.edu/crsc/reports/reports99.html_ (1999)

[3] S.C. Beeler, G.M. Kepler, H.T. Tran, and H.T. Banks. "Reduced Order Modeling and Control of Thin Film Growth in a HPCVD Reactor." Center for Research in Scientific Computation, North Carolina State University, Technical Report CRSC-TR00-33, _http://www.ncsu.edu/crsc/reports/reports00.html_ (2000)

[4] Bortz, D.M., A.D. Rubio, H.T. Banks, A.B. Cain, and R.C. Smith. "Reduced Order Modeling in Control of Open Cavity Acoustics." Center for Research in Scientific Computation, North Carolina State University, Technical Report CRSC-TR00-18, _http://www.ncsu.edu/crsc/reports/reports00.html_ (2000)

[5] del Rosario, R.C.H., H.T. Tran and H.T. Banks. "Proper Orthogonal Decomposition Based Control of Transverse Beam Vibrations: Experimental Implementation." Center for Research in Scientific Computation, North Carolina State University, Technical Report CRSC-TR99-43, _http://www.ncsu.edu/crsc/reports/reports99.html_ (1999)

[6] Kepler, G.M., R.B. Richardson, K.T. Morgan, and J.S. Kimbell. "Computer simulation of inspiratory nasal airflow and inhaled gas uptake in a rhesus monkey." _Toxicol. Appl. Pharmacol._ submitted.

[7] Kepler, G.M., H.T. Tran, and H.T. Banks. "Compensator Control for Chemical Vapor Deposition Film Growth

Using Reduced Order Design Models." Center for Research in Scientific Computation, North Carolina State University, Technical Report CRSC-TR99-41, *http://www.ncsu.edu/crsc/reports/reports99.html* (1999).

[8] Kepler, G.M., H.T. Tran, and H.T. Banks. "Reduced Order Model Compensator Control of Species Transport in a CVD Reactor." Center for Research in Scientific Computation, North Carolina State University, Technical Report CRSC-TR99-15, *http://www.ncsu.edu/crsc/reports/reports99.html* (1999)

[9] Kirby, M. and L. Sirovich. "Application of the Karhunan-Loève Procdure for the Characterization of Human Faces." *IEEE Transactions of Pattern Analysis and Machine Intelligance* **12**,103-108 (1990).

[10] Kimball, J.S., E.A. Gross, D.R. Joyner, M.N. Godo, and K.T. Morgan. "Application of computational fluid dynamics to regional dosimetry of inhaled chemicals in the upper respiratory tract of the rat." *Toxicol. and Appl. Pharmacol.* **121**, 253-263 (1993).

[11] Ly, H.V. and H.T. Tran. "Modeling and control of physical processes using proper orthogonal decomposition." *Mathematical and Computer Modelling* **33**, 223-236 (2001).

[12] Ly, H.V. and H.T. Tran. "Proper orthogonal decomposition for flow calculations and optimal control in a horizontal CVD reactor." Center for Research in Scientific Computation, North Carolina State University, Technical Report CRSC-TR98-13, *http://www.ncsu.edu/crsc/reports/reports98.html* (1998).

[13] Sirovich, L. and M. Kirby. "Low-dimensional Procedure for the Characterization of Human Faces." *Journal of the Optical Society of America* 4, 519-524 (1987).

[14] Subramaniam, R., R.B. Richardson, R. Guilmette, K.T. Morgan, and J.S. Kimbell. "Computational fluid dynamics simulations of inspiratory airflow in the human nose and nasopharynx." *Inhalation Toxicology* 10, 91-120 (1998).

DEFENSE TECHNICAL INFORMATION CENTER
ATTN: DTIC-OCA (ACQUISITION)
8725 JOHN J. KINGMAN ROAD, SUITE 0944
FT. BELVOIR VA 22060-6218

NAVAL AIR WEAPONS CENTER
ATTN: DR. DAVE BURDICK
CODE 472EOOD
CHINA LAKE CA 93555-6001

COMDR, U.S. ARMY AVIATION AND MISSILE COMMAND
ATTN: AMSAM-RD-MG-SP (DR. PAUL RUFFIN)
REDSTONE ARSENAL AL 35898-5241

IIT RESEARCH INSTITUTE/GACIAC
10 WEST 35TH STREET
CHICAGO IL 60616-3799

EGLIN AFB OFFICES:

AFRL/MN/CA-N
AFRL/MNOC-1 (STINFO Office)
AFRL/MNG   **(2 copies)**
AFRL/MNGG
AFRL/MNGI
AFRL/MNGN
AFRL/MNGS
AFRL/MNA
AFRL/MNM

ONE COPY OF EACH UNLESS OTHERWISE SPECIFIED

NOTICE

WHEN GOVERNMENT DRAWINGS, SPECIFICATIONS, OR OTHER DATA ARE USED FOR ANY PURPOSE OTHER THAN IN CONNECTION WITH A DEFINITE GOVERNMENT-RELATED PROCUREMENT, THE UNITED STATES GOVERNMENT INCURS NO RESPONSIBILITY OR ANY OBLIGATION WHATSOEVER. THE FACT THAT THE GOVERNMENT MAY HAVE FORMULATED OR IN ANY WAY SUPPLIED THE SAID DRAWINGS, SPECIFICATIONS, OR OTHER DATA IS NOT TO BE REGARDED BY IMPLICATION, OR OTHERWISE IN ANY MANNER CONSTRUED, AS LICENSING THE HOLDER, OR ANY OTHER PERSON OR CORPORATION; OR AS CONVEYING ANY RIGHTS OR PERMISSION TO MANUFACTURE, USE, OR SELL ANY PATENTED INVENTION THAT MAY IN ANY WAY BE RELATED THERETO.

Small Business Innovation Research Program (SBIR)
DATA RIGHTS LEGEND
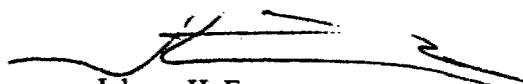Contract Number: F08630-0-1-0010
Contractor: Center for Research in Scientific Research, North Carolina State University

This technical report is releasable to the National Technical Information Services (NTIS). At NTIS it will be available to the general public, including foreign nations.

This technical note has been reviewed for technical content and assessed to be accurate. Due to extenuating circumstances, it is not practical to edit this report for format and it is, therefore, approved "as submitted by the contractor."

LtCol Maria L. Schreffler
Deputy Division Chief
Advanced Guidance Division

Johnny H. Evers
Program Manager
Advanced Guidance Division

Anyone having need of a copy of this report should first contact the Defense Technical Information Center (DTIC) at the address shown below. If you are a registered DTIC User and qualify as a recipient of this document, DTIC can provide you with a copy. Please do not request copies from the Air Force Research Laboratory, Munitions Directorate. Requests for additional copies should be directed to:

Defense Technical Information Center (DTIC)
8725 John J. Kingman Road, Ste 0944
Ft Belvoir, VA 22060-6218

This report is published in the interest of the scientific and technical information exchange. Publication of this report does not constitute approval or disapproval of the ideas or findings. Do not return copies of this report unless contractual obligations or notice on a specific document requires its return. If your address has changed, if you wish to be removed from our mailing list, or if your organization no longer employs the addressee, please notify AFRL/MNG, Eglin AFB FL 32542-6810, to help us maintain a current mailing list. Do not return copies of this report unless contractual obligations or notice on a specific document requires that it be returned..